ARTICLE

Check for updates

Seismic evidence for a thermochemical mantle plume underplating the lithosphere of the Ontong Java Plateau

Takehi Isse [1✉], Daisuke Suetsugu[2], Akira Ishikawa [3], Hajime Shiobara[1], Hiroko Sugioka [4], Aki Ito [2], Yuki Kawano [1], Kazunori Yoshizawa [5], Yasushi Ishihara[2], Satoru Tanaka [2], Masayuki Obayashi [2], Takashi Tonegawa [2] & Junko Yoshimitsu[2]

The Ontong Java Plateau in the western Pacific Ocean is the world's largest oceanic plateau. It was formed 122 million years ago by a massive volcanic event that significantly affected Earth's environment. The cause of the magmatic event remains controversial because the upper mantle structure beneath the plateau is poorly known. Here we use passive seismic data obtained through seafloor observations, alongside existing seismic data, to determine the three-dimensional radially anisotropic shear wave velocity to depths of up to 300 km. We find that the lithosphere–asthenosphere boundary is approximately 40 km deeper beneath the centre of the Ontong Java Plateau than beneath the surrounding seafloor. Based on our results and petrological and rheological constraints, we propose that the lithosphere–asthenosphere boundary has deepened as a result of underplating of dehydrated residual material beneath the pre-existing lithosphere during formation of the Ontong Java Plateau by a thermochemical mantle plume.

---

[1] Earthquake Research Institute, the University of Tokyo, Tokyo, Japan. [2] Research Institute for Marine Geodynamics, Japan Agency for Marine-Earth Science and Technology (JAMSTEC), Yokosuka, Japan. [3] Department of Earth and Planetary Sciences, Tokyo Institute of Technology, Tokyo, Japan. [4] Graduate School of Science, Kobe University, Kobe, Japan. [5] Faculty of Science, Hokkaido University, Sapporo, Japan. ✉email: tisse@eri.u-tokyo.ac.jp

The Ontong Java Plateau (OJP) in the western Pacific Ocean is the largest oceanic Large Igneous Province (LIP) on Earth[1], with crust 30–40 km thick[2–4]. While the entire OJP is thought to have been emplaced at approximately 122 Ma by a single massive magmatic event, influencing the global climate, as well as causing oceanic anoxic events and the extinction of marine species[1], the cause of the magmatism is still debated. The geochemistry of OJP basalts is extraordinarily homogeneous[5], which differs from those of other LIPs and hotspots. The main OJP emplacement was submarine at depths greater than 800 m below sea level[6], but partly subaerial[7], and post-emplacement subsidence has been minimal compared to normal seafloor[8].

Three major hypotheses have been proposed for the origin of the OJP to explain these characteristics: (1) the ascent of a hot mantle plume[1,9,10] with a potential temperature (T_p) higher than 1500 °C; (2) passive mantle upwelling near a spreading ridge[11]; and (3) a meteorite impact resulting in extensive melting[12]; however, none of these hypotheses satisfy existing data or are conclusive. Identifying the origin of the OJP is not only essential to understand Cretaceous Earth geodynamics, but also to evaluate the magnitude and mechanism of a change in the climate that may be induced by a future massive magmatic event. The seismic structure beneath the OJP may be the key to resolving its origin. For example, a recent study[13] found strong radial anisotropy just beneath the Moho at the Hikurangi Plateau, which may have been a part of the single Ontong Java–Manihiki–Hikurangi Plateau[14], with interpretations of its formation via a plume. Current knowledge on the structure beneath the OJP is sparse, particularly for the upper mantle, and seismic studies to date have yielded no direct evidence of a plume. Until now only two studies have focused on the upper mantle beneath the OJP, and the resulting models differ markedly. One study suggests the presence of a low-velocity, rheologically strong mantle root extending as deep as 300 km beneath the entire OJP[15]. Shear wave splitting analysis around the OJP also supports this mantle root hypothesis[16]. More recently, a very high-velocity and compositionally different mantle has been proposed, extending to a depth of 100 km beneath the corner of the L-shaped OJP[17], with no noticeable low-velocity anomalies. These opposing results may arise from the data used, which are solely from land stations well beyond the boundaries of the submarine OJP. To investigate the OJP's upper mantle more reliably, in situ seismic seafloor observations are required.

From late 2014 to early 2017, we conducted the first broadband seismic and electromagnetic investigation of the OJP using the 'OJP array'[18] on OJP and adjacent seafloor and neighbouring islands (Fig. 1). Here, we determine the three-dimensional radially anisotropic shear wave structure of the upper mantle in and around the OJP via surface wave tomography using seismograms recorded by the OJP array and data from existing land and seafloor stations (Supplementary Fig. 1).

Results

Seismic structure. The shear velocity model obtained in this study shows that a high-velocity lid (4.45–4.6 km s^{-1}) at a depth of ~100 km in most regions overlies low-velocity regions at ~150 km depth. This feature is seismic evidence of plate tectonics, i.e., the cold, rigid oceanic lithosphere overlies the hot, weak, viscous, and ductile asthenosphere. However, under the central OJP, the high shear velocity region (4.45–4.6 km s^{-1}, 2% high-velocity anomalies at a depth of 150 km) extends to 150 km, a remarkable feature of the upper mantle. Radial anisotropy is weak ($\xi \equiv (\beta_H/\beta_V)^2 \approx 1.0$) and strong ($\xi > 1.1$) in the lithosphere and asthenosphere, respectively (Figs. 2 and 3), which is similar to normal Pacific Ocean upper mantle[19,20], but the depth of the lithosphere–asthenosphere boundary (LAB) is significantly greater beneath the OJP. The LAB depth, defined here as the depth of the negative peak in the vertical velocity gradient (see Methods, Fig. 3a), is ~130 km, which is much deeper than the average LAB depth (80–90 km) beneath Pacific Ocean seafloor of a similar age in the study region as estimated from surface wave analysis[20]. The LAB depth beneath the OJP is deeper than the deepest LAB previously reported in the Pacific Ocean, i.e., 120 km in the northwest Pacific based on SS precursor analysis[21].

The Nauru Basin, east of the OJP, has a LAB depth of 90 km, similar to the average depth of the LAB in the Pacific Ocean. North of the OJP is an east–west trending low-velocity region (4.35–4.45 km s^{-1}, 0.5–1% low-velocity anomalies, Fig. 3b) with depths of at least 250 km along the Caroline Islands. Radial anisotropy is strong ($\xi > 1.1$) at depths shallower than 150 km. The LAB depth is 70 km, which is consistent with the findings of a previous study that analysed SS precursors[22]. These features may be related to the Caroline plume, which is thought to be present below the easternmost Caroline Islands. The depth of the LAB gradually thins to the east, while thinning to the north and southeast of the OJP is abrupt (Fig. 3a, c, and e). As the crustal thickness of the central OJP is 30–40 km and that of the Nauru Basin is 10 km[23,24], the lithospheric mantle is ≥20 km thicker beneath the OJP than beneath the Nauru Basin. However, owing to limited depth resolution and the definition of the LAB depth
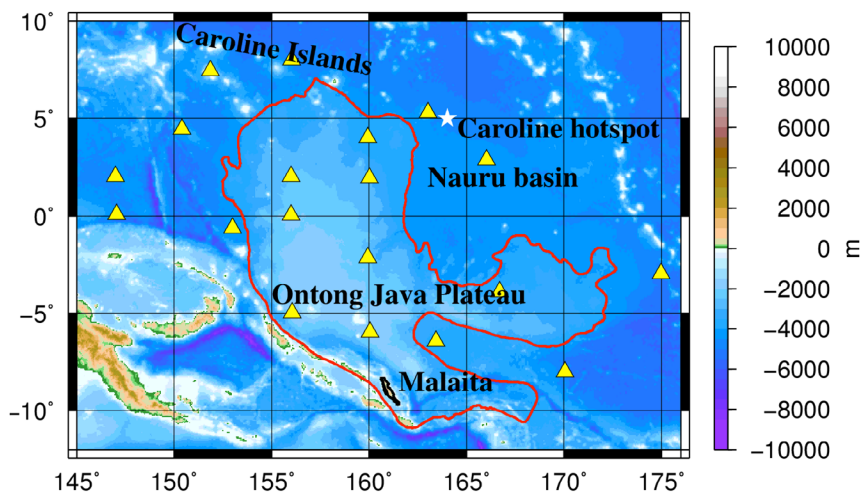

Fig. 1 Bathymetric map of the study region with the locations of the seismic stations indicated. The maps show the OJP[6] (red line), OJP array stations used in this study (yellow triangles), Caroline hotspot[59] (white star), and Malaita Island (black line).
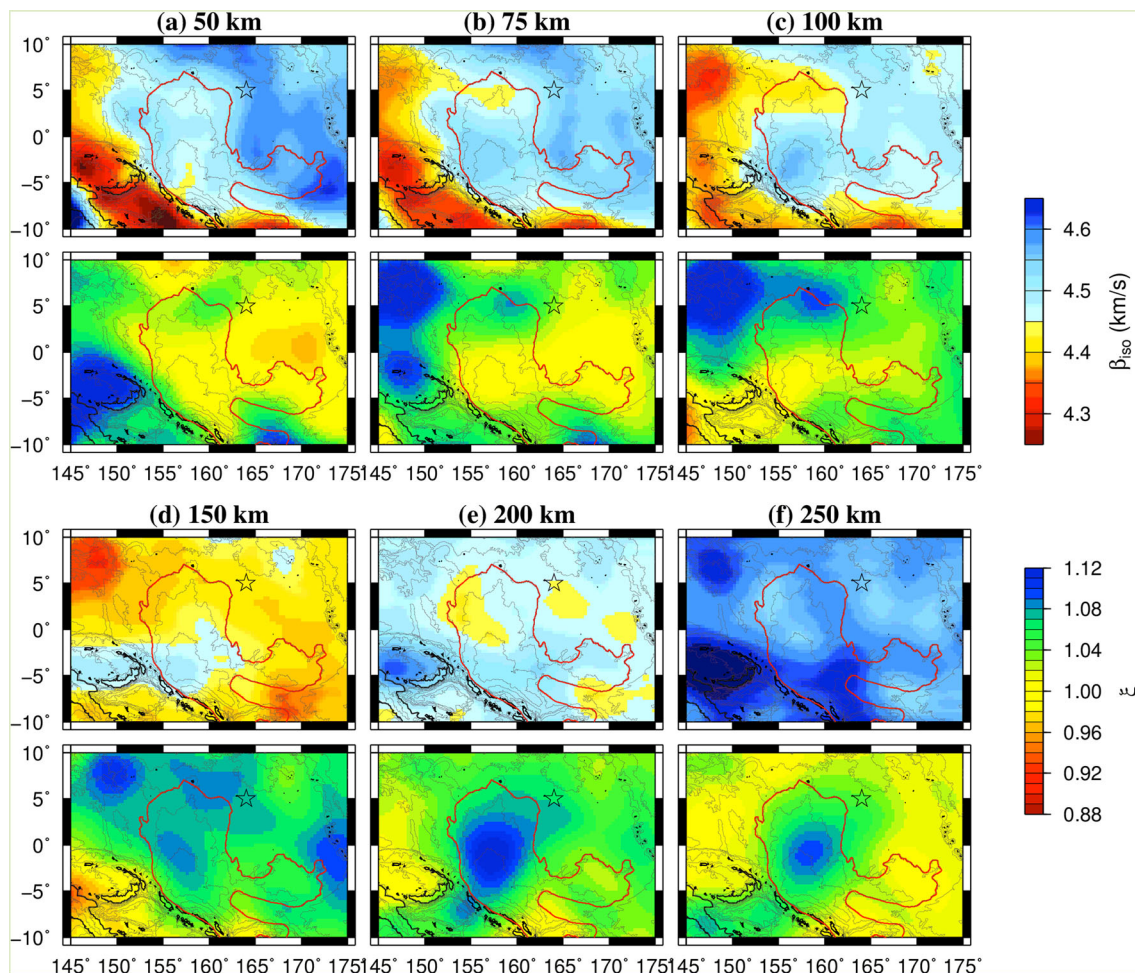
Fig. 2 Shear-wave tomography model. The upper panels show the Voigt-averaged shear wave velocity (β_{iso}) structure and the lower panels show the radial anisotropy ($\xi = (\beta_H/\beta_V)^2$) at depths of **a** 50, **b** 75, **c** 100, **d** 150, **e** 200, and **f** 250 km. Open star shows the Caroline hotspot.

adopted in this study, the LAB depth beneath the OJP may be underestimated by 20 km or more (see Methods, Supplementary Note 1, and Supplementary Fig. 2). The observation of thick lithosphere is possible with multi-mode surface wave tomography, as the first higher-mode Rayleigh wave travelling through the OJP exhibits high phase velocities, which is sensitive to shear wave velocities at a depth of ~100 km and insensitive to those at crustal depths (see Supplementary Note 2 and Supplementary Figs. 3 and 4). Thick lithosphere beneath the OJP is qualitatively consistent with weak seismic attenuation in the OJP mantle[25,26].

Discussion

Thermal versus compositional factors. What is the origin—thermal and/or compositional—of the thick lithosphere beneath the OJP? If thermal effects are the cause, the thick lithosphere, with high-velocity anomalies of ~1–2%, should be accompanied by lower temperature anomalies of ~100–200 K[20] compared to lithosphere beneath the Nauru Basin. One possibility is a difference in lithospheric ages between the OJP and Nauru Basin; according to a half-space cooling model[27], the age of the OJP lithosphere should be ~40 Ma older than that of the Nauru Basin (~130–160 Ma[23]) to account for the temperature difference. However, interpreted seafloor ages underlying the southernmost OJP are ~160 Ma[28] and of the OJP's uppermost crust ~122 Ma[12], which are unlikely to have caused such a large temperature difference. Other cooling models[29] provide even smaller

temperature differences. Another possibility is the existence of small-scale downwelling flow[30] in the asthenosphere beneath the OJP. However, it appears unrealistic that a localised downwelling flow has moved with the OJP and maintained a cool lithosphere. Strong radial anisotropy beneath the OJP lithosphere at depths >150 km indicates the existence of horizontal flow rather than vertical flow. Therefore, we propose that the cause of the thick lithosphere is compositional, which agrees with studies of xenoliths sampled from the Malaita Island where OJP crust has been obducted[9,28,31–34] (Fig. 1). This xenolith population comprises diverse suites of peridotites and garnet pyroxenites that represent virtually the entire section beneath the southern margin of OJP lithosphere, extending to depths of ≤120 km. The upper part (<80 km) of OJP lithosphere is mainly composed of fertile lherzolites originating from pre-existing oceanic lithosphere with subordinate pyroxenitic dykes or sills, whereas the deeper part of the OJP lithosphere, at depths between 90 and 120 km, can be interpreted as melt residues of a mixed peridotite-pyroxenite source from a thermochemical mantle plume[9]. Based on petrological calculations, shear wave velocities of the peridotite beneath the OJP at depths of 60–120 km are estimated to range between 4.6 and 4.5 km s^{-1}, respectively[31], which is consistent with our seismological results of this study (Supplementary Fig. 5). The petrological model does not involve anomalous velocity structures, as proposed by previous studies, such as a broad low-velocity anomaly (4.0–4.1 km s^{-1}) at depths from 80 to 150 km[15] or very high anomalies (4.75 km s^{-1}) extending to a depth of
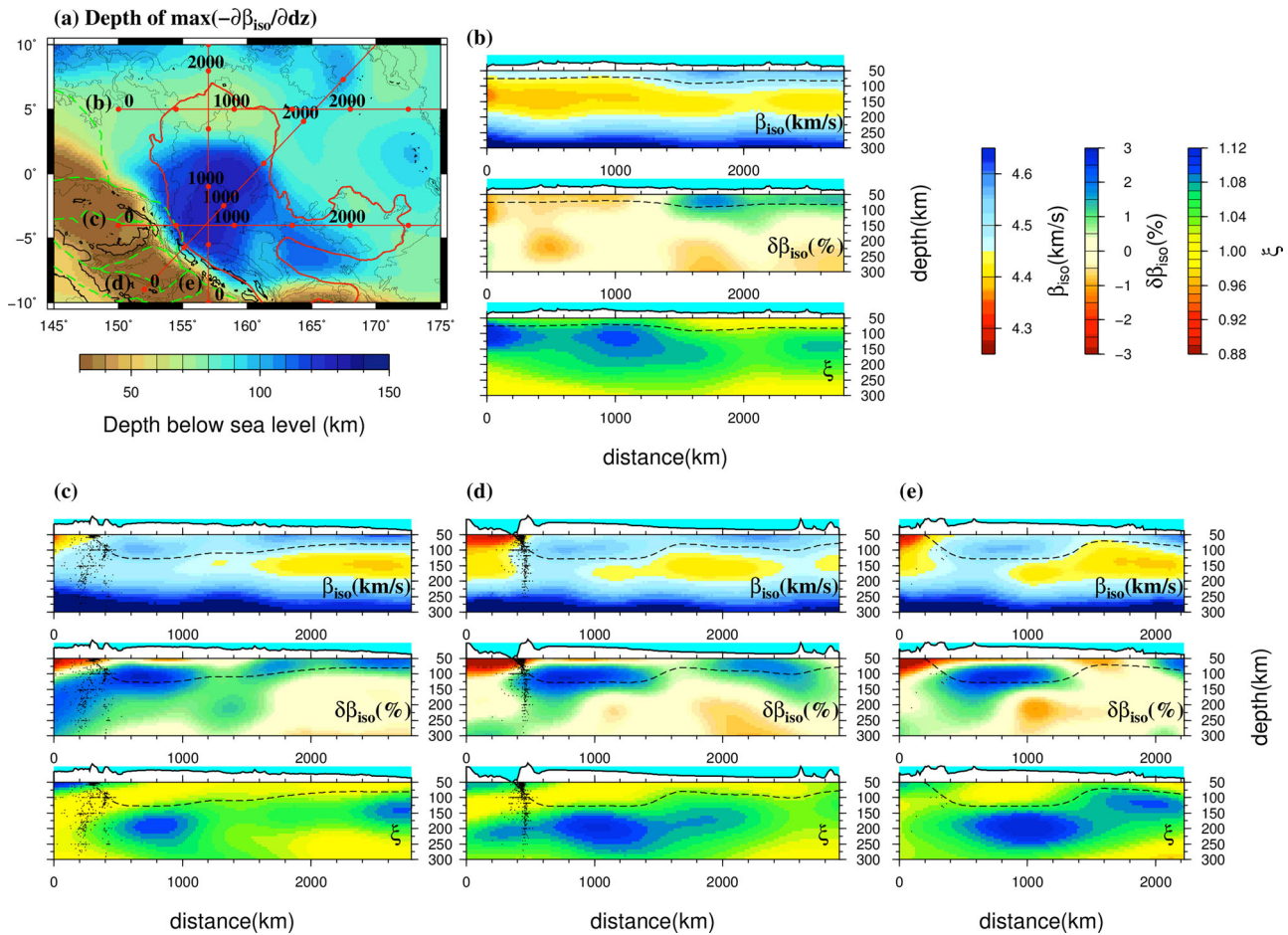
Fig. 3 Estimated depth of the LAB and vertical profiles of the OJP. a Map of LAB depths beneath the OJP and the adjacent region estimated using the negative peak depth of the vertical gradient of β_{iso}. The green dashed line shows the plate boundary. **b–e** Vertical profiles of the shear wave velocity, its anomalies with respect to the average of the studied region, and radial anisotropy along the profiles indicated in **a**. Black dashed lines show the depth of the LAB. Black dots in **b–e** show earthquakes whose magnitudes greater than 4.0 in 1964–2020[60] adjacent to the cross-sections.
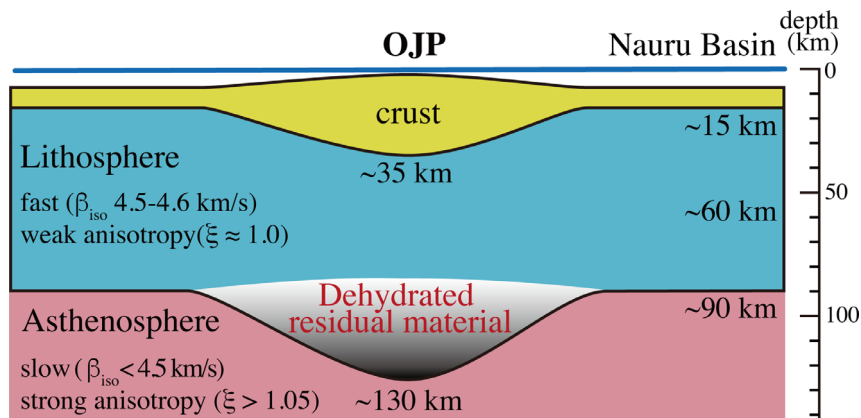

Fig. 4 Schematic illustration of OJP upper mantle. Thick lithosphere (~130 km) exists beneath the centre of the OJP. Dry melt residues underplate pre-existing lithosphere beneath the OJP.

100 km[17]. We consider the seismic structure described here to be more reliable than any structure previously published because our imaging is the first to be based on in situ data from the OJP. Therefore, we conclude that the seismically determined velocity model presented here is consistent with the petrologically determined velocity model, such that the thickened lithosphere was most likely caused by underplating of melt residues of a

thermochemical mantle plume beneath pre-existing oceanic lithosphere at the time of OJP emplacement (Fig. 4).

The arrival of a hot and buoyant mantle plume comprising anhydrous peridotite at the base of the lithosphere should result in considerable subaerial volcanism[11], which is inconsistent with the observation that the main OJP emplacement was submarine[6]. However, a thermochemical plume[35], assuming the incorporation

of compositionally dense but fusible material such as eclogites or garnet pyroxenites, would decrease both the solidus temperature and net buoyancy flux of the plume, such that a large outpouring of basaltic magma could occur with minor topographic uplift of the OJP.

We speculate that the high potential mantle temperature ($T_p >$ 1500 °C), derived from the geochemistry of OJP basalts[36,37] may be overestimated, as modelled 20–30% melting of homogeneous anhydrous peridotite is not a unique solution for the observed lava compositions. Evidence to date shows that OJP basalts are extraordinarily homogeneous[5], depleted in incompatible trace elements including H_2O and CO_2[5,35], and slightly enriched in platinum-group elements (PGEs)[38] compared with other LIPs and hotspots thought to be generated by melting of hetero-geneous plume sources. However, such observations in favour of the OJP magma source being homogeneous anhydrous peridotite remain controversial and inconclusive. Indeed, previous studies[11,39] have pointed out that the high-Ni compositions of olivine from primitive OJP lavas are not compatible with the melting products of common peridotites. This led to the proposal of olivine-free lithology as a more appropriate source for the OJP lavas such as pure eclogite[11] or hybrid pyroxenite formed from reaction between eclogite-derived Si-rich melts and peridotite[39].

We favour the latter because a series of hybrid pyroxenites is the main constituent of deeply derived xenoliths found in Malaita[9,32,33]. Moreover, it would be possible to reconcile the observed chemical and isotopic variations of OJP lavas if the hybridisation process during plume ascent created almost uniform pyroxenite as the main magma source[39]; the melting of hybrid pyroxenite could enhance the release of compatible elements such as Ni and PGEs into the melt, resulting in elevated concentrations of Ni and PGEs in OJP lavas; and the olivine-free but pyroxene-rich residues left behind after the melting of hybrid pyroxenite could accommodate substantial amounts of incompatible trace elements that may account for incompatible element depletion in the primitive OJP magma.

Currently, geochemical modelling of trace element abundances and isotopic compositions of the OJP lavas is challenging because the compositional variability expected for recycled eclogites and resulting hybrid pyroxenites cannot be tightly constrained. This is partly because almost all OJP geochemistry is based on limited data obtained from the uppermost 3–4 km section of erupted lavas, presumably after effective mixing in large magma chambers in an already thickened crust. Nevertheless, a compositionally and isotopically enriched type of basalt was recognised as an overlying veneer of the main group of basalts at several localities, which seems consistent with the more fusible components in the heterogenous plume that was tapped during the waning phases of the OJP magmatism[36,40]. Future sampling of significantly deeper crustal sections[41] could clarify the extents of the heterogeneities in OJP lavas, which is required for viable trace element modelling and T_p estimates for the thermochemical plume[35].

Other hypotheses, such as the passive upwelling of dense material[11] and a meteorite impact[12], which do not invoke deep mantle plume activity for the formation of the OJP, are consistent with the lack of convincing evidence of a post-OJP hotspot track (plume tail). The Louisville seamount trail is a potential plume trail[42] but remains controversial. However, the thickened litho-sphere observed in this study is difficult to reconcile with these non-plume scenarios. In the passive upwelling hypothesis, basaltic magma would have been produced by almost complete melting of recycled crustal material that ascended via astheno-spheric upwelling near a spreading ridge. This appears unlikely to have produced melt residues sufficient to thicken the OJP lithosphere as this essentially prevents the melting of anhydrous peridotite under high-pressure conditions. For impact-induced

melting, basaltic magma would have been largely supplied first from the uppermost ~150 km of pre-existing crust and mantle beneath the impact site where the most decompression and shock/release wave melting would have occurred[43], although an extended secondary episode of additional melting would occur at greater depths[44]. However, if the melting region were sufficiently large to thicken the vast area of OJP lithosphere, Jurassic-aged oceanic crust and mantle identified in the Malaita xenolith population should have been disturbed[28], which has not been observed. A lack of extraterrestrial signatures in coeval Pacific marine sediments would also suggest no impact event at the time of OJP formation[34]. We consider impact hypothesis to be unlikely, although absence of evidence does not equate to evidence of absence.

How can melt residues survive for over 120 Ma? During the formation of OJP crust, the volatile components of the plume, including H_2O were incorporated into the basaltic melt, resulting in dry[45] and rheologically strong[46] residual plume material. The restite root hypothesis[47], which assumes that a dry, hot, highly viscous restite root attached itself beneath the hotspot lithosphere, yielding a thick high-viscosity layer (lithosphere), was proposed to explain hotspot swell uplift. Recent receiver function analysis suggests that the LAB is as deep as 100 km beneath hotspot islands in the Pacific Ocean[48], which is similar to the deep LAB beneath the OJP. Recent rheological and geophysical studies[49,50] indicate that the asthenosphere is wet and thus rheologically weak compared to the lithosphere, which suggests that the dry and rigid melt residues could have moved with Pacific lithosphere over long time intervals. A similar mechanism has been proposed to explain the extended life of continental cratons (>2 Gyr)[51].

The area of >20 km thicker lithosphere beneath the OJP is ~5×10^5 km^2, so that the volume of the dry, dense residue that we have identified is ~$1–2 \times 10^7$ km^3, which is significantly less than the mantle source volume estimated to form OJP crust ($1–3 \times 10^8$ km^3)[35]. One possible explanation is that most residue moved laterally and did not underplate during emplacement and the last residue formed thick lithosphere during the waning phase of activity. An alternative explanation is that most dense residue has delaminated while the OJP has moved with Pacific lithosphere after emplacement. The latter explanation may be more plausible given that this might explain the less-than-predicted subsidence of OJP seafloor.

Methods
We employed a surface wave tomography method consisting of three independent stages[20,52,53]. First, we measured the path-specific multimode phase-velocity dispersion curves of Love and Rayleigh waves from the fundamental to the 4th higher mode using a fully nonlinear waveform inversion method. The waveform-fitting process was fully automated, where the quality of the obtained dispersion curves was evaluated by a reliability parameter and determined by the degree of waveform fitting and relative power of each mode in the selected bandpass filtered time window. This empirical criterion is identical to that of our previous study[20]. We obtained, at most, 2000–4000 phase velocity dispersion curves for the fundamental Rayleigh waves, and 500–1500 for the higher modes in the 5–30 mHz frequency range. For the Love waves, the number of dispersion curves was approximately half the number obtained for the Rayleigh waves. Approximately 5–10% and 20–30% of the Love and Rayleigh wave dispersion curves, respectively, were obtained from broadband ocean bottom seismographs (BBOBSs). For the second stage, we inverted the path-specific multimode phase velocities for two-dimensional phase-velocity mapping at each frequency, incorporating finite-frequency and ray-bending effects. Phase velocity maps were expanded in a set of B-spline functions with a rectangular grid, with the interval in each map varying from 2° to 6.5° depending on the number of paths and the size of the Fresnel zone for each mode and frequency. Finally, we inverted the multimode phase velocity maps to generate a three-dimensional radially anisotropic shear wave velocity model, employing iterative least-squares inversion. The use of up to the 4th higher modes of surface waves enables us to improve the depth resolution of the radial anisotropy (Supplementary Fig. 6).

Following the protocol introduced in our previous study[20], we used β_V and β_H as independent parameters, showing β_{iso}, which is the Voigt-averaged isotropic shear wave velocity, where $\beta_{iso}^2 = (2/3)\beta_V^2 + (1/3)\beta_H^2$ and $\xi = (\beta_H/\beta_V)^2$. In this

inversion, two a priori parameters control the degree of perturbation and smoothness in the depth variations—the standard deviation, σ, and correlation length, L—which were respectively set to $0.01\ \mathrm{km\ s^{-1}}$ and 3 km in the crust, $0.04\ \mathrm{km\ s^{-1}}$ and 15 km between the Moho and a depth of 400 km, and $0.03\ \mathrm{km\ s^{-1}}$ and 15 km between depths of 400 and 670 km. Here, σ decreases linearly from $0.03\ \mathrm{km\ s^{-1}}$ at 670 km to $0.02\ \mathrm{km\ s^{-1}}$ at 1,500 km, while L increases from 15 km at a depth of 670 km to 30 km at a depth of 1500 km. We confirmed L and σ through a series of synthetic tests, in which L and σ were varied to observe whether the retrieved models were consistent with various input models. Our one-dimensional initial velocity model was modified from PREM by smoothing the 220 km discontinuity with corrections for the crustal structure using the CRUST1.0 model and a recent result[4] from receiver function analysis beneath the OJP (Supplementary Fig. 7). We corrected for the anelastic effect using the attenuation model of PREM with a reference frequency of 1 Hz. The Moho depth of an initial model was fixed during the inversion. The mislocation of the Moho depth affected the inverted structure (Supplementary Note 3 and Supplementary Fig. 8); the obtained structure shallower than ~50 km was less resolved because the phase velocities we used were longer than 30 mHz, which is less sensitive in shallow depths (See Supplementary Fig. 4d). Checkerboard resolution tests suggested that the lateral resolution of the OJP is ~4° for the isotropic structure and ~7° for the anisotropic structure (Supplementary Fig. 9). We applied a spatial two-dimensional FFT low-pass Gaussian filter at 4° and 7° (grdfft in GMT[54]). As the sensitivity of surface waves decrease with depth, we only show a three-dimensional radially anisotropic shear wave velocity structure for depths shallower than 300 km. We also performed a synthetic test to assess the influence of the subducting slab south of the OJP, which is indicated as a fast velocity anomaly. The recovered model suggested that the fast subducting slab anomalies have little effect on the mantle structure beneath the OJP (Supplementary Fig. 10)

A popular method for analysing the LAB is to use a reflected or converted seismic wave. In the northern part of the OJP, the depth of LAB is estimated to be ~70 km based on SS-precursor wave analysis[22]. However, SS-precursor waves do not sample the main part of the OJP due to the locations of the seismic stations and earthquakes. While S-wave receiver function analysis is also a common method for estimating the LAB depth[55], a high level of horizontal component noise in the OJP array data prevents this type of analysis. Alternatively, we propose an approach that uses a negative gradient peak in the shear wave velocity as a proxy for the LAB depth. For this, we calculated the depth of the negative peak in the vertical gradient of the shear wave velocity obtained from the tomographic model to analyse the lateral variation of LAB depth. From a seismological perspective, the upper mantle structure can be described as a high-velocity lid (lithosphere) overlying the low-velocity zone (asthenosphere), such that the negative peak in the vertical gradient can be used as a proxy for the LAB[20,53,56]. Thus, we defined the depth of the proxy as the depth of the LAB. To assess the depth resolution of the surface waves and the reliability of this proxy, we performed synthetic tests using a synthetic shear wave velocity model and by changing the thickness of a 3% high-velocity lid (Supplementary Note 1 and Supplementary Fig. 2). The recovered vertical profiles show a high-velocity lid at the top and a low-velocity body below. Although the sharp discontinuity was not recovered because surface waves are insensitive to this, the peak depth represents the depth of the discontinuity (i.e., LAB) for input LAB depths of 70–110 km within an accuracy of 15 km. The peak depths are greater than the input discontinuity depths for depths of 60–80 km and shallower for depths of 90–160 km, indicating that the deep LAB beneath the OJP is likely to be underestimated by 20 km or more whereas this is not the case for the surrounding regions (e.g., Nauru and Caroline).

Data. We collected seismic waveform data recorded by the OJP array for earthquakes with moment magnitudes (Mw) greater than 5.5 in the western Pacific Ocean to analyse the upper mantle shear wave structure beneath the OJP. As these data alone do not suffice for this purpose, we also collected seismic data recorded on land and on the seafloor in the western Pacific Ocean (Supplementary Fig. 1). These data are distributed by the Ocean Hemisphere network Project (OHP) and the Incorporated Research Institutions for Seismology Data Management Center (IRIS DMC), which were collected for earthquakes between 1990 and 2016. The study region in the western Pacific Ocean is similar to that of another recent study[17] in which only seismic data from land stations were used. Here, we used seafloor observation data recorded by BBOBSs as well as land data from a total of 161 stations, of which 115 are BBOBS stations (Supplementary Fig. 1). Vertical component seismograms recorded on the seafloor are contaminated by tilt noise caused by leaks of a high degree of noise in the horizontal components induced by seafloor currents[57] and compliance noise induced by the infragravity waves that are also recorded by seafloor pressure data[58]. We removed this noise from the BBOBS station data in the OJP array by applying a spectral transfer function between the vertical and horizontal components and between the vertical and pressure components, respectively.

Data availability
The tomography model (OJP-S-isse) used in this study is available in the Researchgate repository (https://www.researchgate.net/publication/351061906_OJP-S-Isse, https://doi.org/10.13140/RG.2.2.29857.94561/1) and in the supplementary data 1.

References
1. Coffin, M. F. & Eldholm, O. Large igneous provinces: crustal structure, dimensions, and external consequences. *Rev. Geophys.* **32**, 1–36 (1994).
2. Furumoto, A. S., Webb, J. P., Odegard, M. E. & Hussong, D. M. Seismic studies on the Ontong Java Plateau, 1970. *Tectonophysics* **34**, 71–90 (1976).
3. Gladczenko, T. P., Coffin, M. F. & Eldholm, O. Crustal structure of the Ontong Java Plateau: modeling of new gravity and existing seismic data. *J. Geophys. Res. Solid Earth* **102**, 22711–22729 (1997).
4. Tonegawa, T. et al. Characterization of crustal and uppermost-mantle seismic discontinuities in the Ontong Java Plateau. *J. Geophys. Res. Solid Earth* **124**, 7155–7170 (2019).
5. Tejada, M. L. G., Mahoney, J. J., Duncan, R. A. & Hawkins, M. P. Age and geochemistry of basement and alkalic rocks of Malaita and Santa Isabel, Solomon Islands, Southern Margin of Ontong Java Plateau. *J. Petrol.* **37**, 361–394 (1996).
6. Mahoney, J. J. et al. Proceedings of the Ocean Drilling Program, Vol. 192. *Initial Reports. Basement Drilling of the Ontong Java Plateau.* (2001) https://doi.org/10.2973/odp.proc.ir.192.2001
7. Thordarson, T. Accretionary-lapilli-bearing pyroclastic rocks at ODP Leg 192 Site 1184: A record of subaerial phreatomagmatic eruptions on the Ontong Java Plateau in *Origin and evolution of the Ontong Java Plateau* (eds: Fitton, J. G. et al.) 133–150 (Geological Society, London, Special Publication 229, 2004).
8. Neal, C. R., Mahoney, J. J., Kroenke, L. W., Duncan, R. A. & Petterson, M. G. The Ontong Java Plateau in *Large Igneous Provinces: continental, oceanic, and planetary flood volcanism* (eds. Mahoney, J. J. & Coffin, M. F.) **100**, 183–216, (AGU, 1997).
9. Ishikawa, A., Maruyama, S. & Komiya, T. Layered lithospheric mantle beneath the Ontong Java Plateau: Implications from xenoliths in Alnöite, Malaita, Solomon Islands. *J. Petrol.* **45**, 2011–2044 (2004).
10. Tejada, M. L. G. et al. Pin- pricking the elephant: Evidence on the origin of the Ontong Java Plateau from Pb-Sr-Hf-Nd isotopic characteristics of ODP Leg 192 basalts in *Origin and evolution of the Ontong Java Plateau* (eds.: Fitton, J. G. et al.) 133–150 (Geological Society, London, Special Publication 229, 2004).
11. Korenaga, J. Why did not the Ontong Java Plateau form subaerially? *Earth Planet. Sci. Lett.* **234**, 385–399 (2005).
12. Ingle, S. & Coffin, M. F. Impact origin for the greater Ontong Java Plateau? *Earth Planet. Sci. Lett.* **218**, 123–134 (2004).
13. Stern, T., Lamb, S., Moore, J. D. P., Okaya, D. & Hochmuth, K. High mantle seismic P-wave speeds as a signature for gravitational spreading of superplumes. *Sci. Adv.* **6**, eaba7118 (2020).
14. Taylor, B. The single largest oceanic plateau: Ontong Java–Manihiki–Hikurangi. *Earth Planet. Sci. Lett.* **241**, 372–380 (2006).
15. Richardson, W. P., Okal, E. A. & Van der Lee, S. Rayleigh-wave tomography of the Ontong-Java Plateau. *Phys. Earth Planet. Inter.* **118**, 29–51 (2000).
16. Klosko, E. R., Russo, R. M., Okal, E. A. & Richardson, W. P. Evidence for a rheologically strong chemical mantle root beneath the Ontong–Java Plateau. *Earth Planet. Sci. Lett.* **186**, 347–361 (2001).
17. Covellone, B. M., Savage, B. & Shen, Y. Seismic wave speed structure of the Ontong Java Plateau. *Earth Planet. Sci. Lett.* **420**, 140–150 (2015).
18. Suetsugu, D. et al. The OJP array: seismological and electromagnetic observation on seafloor and islands in the Ontong Java Plateau. *JAMSTEC Rep. Res. Dev.* **26**, 54–64 (2018).
19. Nettles, M. & Dziewoński, A. M. Radially anisotropic shear velocity structure of the upper mantle globally and beneath North America. *J. Geophys. Res.* **113**, B02303 (2008).
20. Isse, T. et al. Surface wave tomography for the Pacific Ocean incorporating seafloor seismic observations and plate thermal evolution. *Earth Planet. Sci. Lett.* **510**, 116–130 (2019).
21. Tharimena, S., Rychert, C. A., Harmon, N. & White, P. Imaging Pacific lithosphere seismic discontinuities—Insights from SS precursor modeling. *J. Geophys. Res.* **122**, 2131–2152 (2017).
22. Tharimena, S., Rychert, C. A. & Harmon, N. Seismic imaging of a mid-lithospheric discontinuity beneath Ontong Java Plateau. *Earth Planet. Sci. Lett.* **450**, 62–70 (2016).
23. Mochizuki, K., Coffin, M. F., Eldholm, O. & Taira, A. Massive Early Cretaceous volcanic activity in the Nauru Basin related to emplacement of the Ontong Java Plateau. *Geochem. Geophys. Geosyst.* **6**, Q10003 (2005).

24. Miura, S. et al. Deep seismic investigation of the Ontong Java Plateau. *Eos, Trans. AGU* **92**, 61–62 (2011).
25. Gomer, B. M. & Okal, E. A. Multiple-ScS probing of the Ontong-Java Plateau. *Phys. Earth Planet. Inter.* **138**, 317–331 (2003).
26. Suetsugu, D. et al. High Q ScS beneath the Ontong Java Plateau. *Earth Planets Space* **71**, 97 (2019).
27. Stein, C. A. & Stein, S. A model for the global variation in oceanic depth and heat flow with lithospheric age. *Nature* **359**, 123–129 (1992).
28. Ishikawa, A., Nakamura, E. & Mahoney, J. J. Jurassic oceanic lithosphere beneath the southern Ontong Java Plateau: evidence from xenoliths in alnöite, Malaita, Solomon Islands. *Geology* **33**, 393–396 (2005).
29. Parsons, B. & Sclater, J. G. An analysis of the variation of ocean floor bathymetry and heat flow with age. *J. Geophys. Res.* **82**, 803–827 (1977).
30. Huang, J. & Zhong, S. Sublithospheric small-scale convection and its implications for the residual topography at old ocean basins and the plate model. *J. Geophys. Res.* **110**, B05404 (2005).
31. Tommasi, A. & Ishikawa, A. Microstructures, composition, and seismic properties of the Ontong Java Plateau mantle root. *Geochem. Geophys. Geosyst.* **15**, 4547–4569 (2014).
32. Ishikawa, A., Kuritani, T., Makishima, A. & Nakamura, E. Ancient recycled crust beneath the Ontong Java Plateau: isotopic evidence from the garnet clinopyroxenite xenoliths, Malaita, Solomon Islands. *Earth Planet. Sci. Lett.* **259**, 134–148 (2007).
33. Ishikawa, A., Pearson, D. G. & Dale, C. W. Ancient Os isotope signatures from the Ontong Java Plateau lithosphere: tracing lithospheric accretion history. *Earth Planet. Sci. Lett.* **301**, 159–170 (2011).
34. Tejada, M. L. G., Ravizza, G., Suzuki, K. & Paquay, F. S. An extraterrestrial trigger for the Early Cretaceous massive volcanism? Evidence from the paleo-Tethys Ocean. *Sci. Rep.* **2**, 268 (2012).
35. Kerr, A. C. & Mahoney, J. J. Oceanic plateaus: Problematic plumes, potential paradigms. *Chem. Geol.* **241**, 332–353 (2007).
36. Fitton, J. G. & Godard, M. Origin and evolution of magmas on the Ontong Java Plateau in *Origin and evolution of the Ontong Java Plateau* (eds.: Fitton, J. G. et al.) 151–178 (Geological Society, London, Special Publication 229, 2004).
37. Herzberg, C. Partial melting below the Ontong Java Plateau in *Origin and evolution of the Ontong Java Plateau* (eds.: Fitton, J. G. et al.) 179–183 (Geological Society, London, Special Publication 229, 2004).
38. Chazey, W. J. & Neal, C. R. Large igneous province magma petrogenesis from source to surface: Platinum-group element evidence from Ontong Java Plateau basalts recovered during ODP Legs 130 and 192 in *Origin and evolution of the Ontong Java Plateau* (eds. Fitton, J. G. et al.) 219–238 (Geological Society, London, Special Publication 229, 2004).
39. Sobolev, A. V. et al. The amount of recycled crust in sources of mantle-derived melts. *Science* **316**, 412–417 (2007).
40. Tejada, M. L. G. et al. Cryptic lower crustal signature in the source of the Ontong Java Plateau revealed by Os and Hf isotopes. *Earth Planet. Sci. Lett.* **377-378**, 84–96 (2013).
41. Sano, T. et al. Testing the Ontong Java Nui Hypothesis: The Largest Supervolcano ever on the Earth. *J. Geography*, **130**, Japanese with English abstract (2021).
42. Mahoney, J. J. & Spencer, K. J. Isotopic evidence for the origin of the Manihiki and Ontong Java oceanic plateaus. *Earth Planet. Sci. Lett.* **104**, 196–210 (1991).
43. Jones, A. P., Wunemann, K. & Price, G. D. Modeling impact volcanism as a possible origin for the Ontong Java Plateau in *Plates, plumes and paradigms* (eds. Foulger, G. R., Natland, J. H., Presnall, D. C. & Anderson, D. L.), 711–720, (Geological Society of America, Special Paper 388, 2005).
44. Elkins-Tanton, L. T., Hager, B. H. & Grove, T. L. Magmatic effects of the lunar late heavy bombardment. *Earth Planet. Sci. Lett.* **222**, 17–27 (2004).
45. Demouchy, S., Ishikawa, A., Tommasi, A., Alard, O. & Keshav, S. Characterization of hydration in the mantle lithosphere: Peridotite xenoliths from the Ontong Java Plateau as an example. *Lithos* **212–215**, 189–201 (2015).
46. Mackwell, S. J., Kohlstedt, D. L. & Paterson, M. S. The role of water in the deformation of olivine single crystals. *J. Geophys. Res. Solid Earth* **90**, 11319–11333 (1985).
47. Yamamoto, M., Phipps Morgan, J. & Morgan, W. J. Global plume-fed asthenosphere flow—I: Motivation and model development in *Special Paper 430: Plates, Plumes and Planetary Processes* 430, 165–188 (Geological Society of America, 2007).
48. Rychert, C. A., Harmon, N. & Tharimena, S. Seismic Imaging of the Base of the Ocean Plates in *Lithospheric discontinuities* (eds. Yuan, H. & Romanowicz, B.) 71–87, https://doi.org/10.1002/9781119249740.ch4 (John Wiley & Sons, 2018).
49. Karato, S. & Park, J. On the origin of the upper mantle seismic discontinuities in *Lithospheric discontinuities* (eds. Yuan, H. & Romanowicz, B.) 5–34, https://doi.org/10.1002/9781119249740.ch1 (John Wiley & Sons, 2018).
50. Yuan, H. & Romanowicz, B. Lithospheric discontinuities. (John Wiley & Sons, 2018). https://doi.org/10.1002/9781119249740.
51. Peslier, A. H., Woodland, A. B., Bell, D. R. & Lazarov, M. Olivine water contents in the continental lithosphere and the longevity of cratons. *Nature* **467**, 78–81 (2010).
52. Yoshizawa, K. & Ekström, G. Automated multimode phase speed measurements for high-resolution regional-scale tomography: application to North America. *Geophys. J. Int.* **183**, 1538–1558 (2010).
53. Yoshizawa, K. Radially anisotropic 3-D shear wave structure of the Australian lithosphere and asthenosphere from multi-mode surface waves. *Phys. Earth Planet. Inter.* **235**, 33–48 (2014).
54. Wessel, P. & Smith, W. H. F. New, improved version of Generic Mapping Tools released. *EOS Trans. AGU* **79**, 579 (1998).
55. Kawakatsu, H. et al. Seismic evidence for sharp lithosphere-asthenosphere boundaries of oceanic plates. *Science* **324**, 499–502 (2009).
56. Burgos, G. et al. Oceanic lithosphere-asthenosphere boundary from surface wave dispersion data. *J. Geophys. Res. Solid Earth* **119**, 1079–1093 (2014).
57. Crawford, W. C. & Webb, S. C. Identifying and removing tilt noise from low-frequency (<0.1 Hz) seafloor vertical seismic data. *Bull. Seismol. Soc. Am.* **90**, 952–963 (2000).
58. Webb, S. C. & Crawford, W. C. Long-period seafloor seismology and deformation under ocean waves. *Bull. Seismol. Soc. Am.* **89**, 1535–1542 (1999).
59. Steinberger, B. Plumes in a convecting mantle: Models and observations for individual hotspots. *J. Geophys. Res.* **105**, 11127–11152 (2000).
60. International Seismological Centre (2020), On-line Bulletin, https://doi.org/10.31905/D808B830.

Acknowledgements

Author contributions

T.I. performed the seafloor observation, analysed the data, and wrote the manuscript. D.S. organised the OJP Array seafloor observation and wrote the manuscript. A.I.S. interpreted and wrote the section on the petrological results. H.S.H., H.S.U., and A.I.T. performed the seafloor observations. Y.K. developed the code for noise reduction of the seismological data. K.Y. developed the code for surface wave analysis. Y.I., S.T., M.O., T.T., and J.Y. organised and performed the island observations. All authors read and approved the final manuscript.

Competing interests

The authors declare no competing interests.

Additional information